Degradation of Methyl Violet over Fenton-Like Hydroxyapatite Catalysts, Kinetics and Thermodynamics Studies

Yasmina Roumila (yas.roumila@gmail.com)
University of Sciences and Technology Houari Boumediene: Universite des Sciences et de la Technologie Houari Boumediene

Djaafar Meziani
University of Sciences and Technology Houari Boumediene: Universite des Sciences et de la Technologie Houari Boumediene

Saadia Debaghi
University of Sciences and Technology Houari Boumediene: Universite des Sciences et de la Technologie Houari Boumediene

Kaïssa Abdmeziem
University of Sciences and Technology Houari Boumediene: Universite des Sciences et de la Technologie Houari Boumediene

Research Article

Keywords: Hydroxyapatite, Fenton like, Environment, Dye pollutant, Kinetic, Thermodynamic

Posted Date: August 13th, 2021

DOI: https://doi.org/10.21203/rs.3.rs-569149/v1

Degradation of Methyl Violet over Fenton-Like Hydroxyapatite Catalysts, Kinetics and Thermodynamics Studies

Yasmina Roumila[1*], Djaafar Meziani[1], Saadia Debaghi[1], Kaïssa Abdmeziem[1]

[1] USTHB, Faculty of Chemistry, Laboratory of Electrochemistry-Corrosion, Metallurgy and Inorganic Chemistry, BP 32 El-Alia, 16111 Algiers, Algeria

Abstract

Hydroxyapatite (HA), a calcium hydroxyphosphate was prepared via precipitation method and used as a catalyst in a Fenton like process for methyl violet (MV) dye degradation. This study is aimed to evaluate the effect of hydrogen peroxide concentration, HA dose, initial pH, temperature and MV concentration on the catalyst performance to find out the optimum conditions leading to maximum efficiency of the Fenton process. The results showed that MV dye with a concentration of 20 mg L^{-1} can be removed within just 10 minutes at the optimal conditions of 36 mmol L^{-1} H_2O_2 and 2.5 g L^{-1} HA at pH of 6.65 and T = 48 °C). The experimental outcome of this study also demonstrates that HA displayed a good recyclability over three cycles; while the use of scavenger highlighted that the hydroxyl radical $HO^{\bullet}$ was the main active species for MV degradation. The catalytic tests result of MV dye degradation were analyzed by the first-order, second-order and Benhnajady-Modirshahla-Ghanbery (BMG) kinetic models, those showing that the Fenton like reaction follows the first-order and BMG models. The activation energy of the reaction and the values of thermodynamic parameters such as standard enthalpy (ΔH^{*0}), entropy (ΔS^{*0}) and Gibbs free energy (ΔG^{*0}) were also evaluated. Those results revealed that the degradation of MV over the as-synthesized material is an endothermic and non-spontaneous process.

Keywords : Hydroxyapatite ; Fenton like ; Environment ; Dye pollutant ; Kinetic ; Thermodynamic

[*] *To whom correspondence should be addressed:*

E-mail yas.roumila@gmail.com , yroumila@usthb.dz

Tel / Fax : +00 213 21 24 73 11 / +00 213 21 24 80 08

1 INTRODUCTION

Water pollution becomes a universal disaster that leads to environmental degradation and declining water quality. The textile industry is an example of the industrial sector where high quantities of water are used in the dyeing process (Lellis et al. 2019). Textile industries produce a lot of wastewater, which contains a number of contaminants, among them various dyes (Wu et al. 2008). Indeed, many dyes are often resistant to biodegradation, hazardous and may even be detrimental at very low concentrations. They affect aquatic life by causing disorders and serious threats to public health (Khan et al. 2014). This is the reason why many researchers in the field of water treatment are interested in the elimination of dye pollutant by adapting several methods such as: coagulation, adsorption, biodegradation, precipitation, membrane separation and advanced oxidation processes (AOPs) (Meziani et al. 2016; Ikhsan et al. 2020; Berkessa et al. 2020; Bilińska et al. 2020; He et al. 2020; Kiani et al. 2020; Mortadi et al. 2020). In recent years, advanced oxidation processes have been studied as a promising kind of treatment method for organic wastewater, based on in situ generation of highly oxidant species, such as hydroxyl radicals ($HO^{\bullet}$, $E_0 = 2.81$ V/NHE) among others (Zaviska et al. 2009). These oxidant species are able to degrade organic pollutants up to complete mineralization. The versatility of AOPs is enhanced by the fact that they offer different possible ways for radical's production**,** thus allowing a better conformity with the specific treatment's requirements.

One of the most frequently used AOPs is the Fenton process, where hydroxyl radical was produced through the reduction of hydrogen peroxide (H_2O_2) by Fe^{2+}. Fenton's reagent is an interesting solution since it allows high depuration levels at room temperature and pressure conditions, using innocuous and easy to handle reactants (Babuponnusami and Muthukumar 2014; Wang et al. 2016). Likewise, the use of iron as a catalyst has major advantages such as: high abundance, environmental compatibility, low toxicity and high reactivity. However, Fenton processes present some limitations such as the requirement of strict pH control ($3 < pH < 4$), and difficulties in the recycling of the homogeneous catalyst leading to high operating cost (Ajoudanian and Nezamzadeh-Ejhieh 2015; Bello et al. 2019). In order to overcome these disadvantages, iron was either complexed with organic molecules, impregnated in different solid catalysts (zeolites, porous carbon and clays)(Gonzalez-Olmos et al. 2011; Hassan and Hameed 2011; Fida et al. 2017; Lan et al. 2020; Long et al. 2020; Zárate-Guzmán et al. 2020; Zhang et al. 2020), or used in oxide form such as goethite (FeOOH), magnetite (Fe_3O_4) and hematite (Fe_2O_3) (Hassan and Hameed 2011; Sebatini et al. 2020; Bilińska et al. 2020; Tang et

al. 2020). Furthermore, materials based on other transition metals were used as heterogeneous Fenton-like catalysts such as metal oxides, metalphosphates and MOFs (Roumila et al. 2016; Zhou et al. 2020; Dong et al. 2021).

Among these types of materials, our attention was focused on metalphosphates. These materials have variable properties, due to their structures, textures and the presence of metals that are considered as active sites involved in catalytic reactions. HA with chemical formula of $Ca_5(PO_4)_3OH$ is a well-known material in metalphosphates family, synthesized in various forms such as powders, micro/nano-crystals, dense or porous blocks/sheets/ceramics. HA is the most stable phase among various calcium phosphates under neutral or basic conditions and it is well known for its bioactivity, biocompatibility, lack of toxicity and excellent surface ion-exchange properties (Venkateswarlu et al. 2010; Fihri et al. 2017). HA is thus used in various fields, it has displayed promising potential in biomedical fields due to its chemical compositional and biological similarity to native tissues (Sangeetha et al. 2018; Riaz et al. 2018; Ciobanu and Harja 2019). It is also applied in other fields of industrial or technological interests such as in different organic reactions as a catalyst (Sebti et al. 2002; Saber et al. 2003; Zahouily et al. 2003), in water purification as a photocatalyst (Nishikawa 2004; Fihri et al. 2017), or as adsorbent for heavy metals like lead and cadmium (Oliva et al. 2011; Oulguidoum et al. 2019; Vahdat et al. 2019) and organic contaminants (Harja and Ciobanu 2018; Ooi et al. 2019).

In this work, we report the synthesis and the characterization of HA obtained by using the precipitation method. The catalytic performances of our material were further investigated in MV dye elimination using heterogeneous Fenton-like process. The effects of various conditions that may influence the catalytic reaction, including hydrogen peroxide concentration, HA dose, dye concentrations, temperature and initial pH of the solution were investigated. The kinetic and thermodynamic studies of MV dye degradation, were also established.

2 MATERIALS AND METHODS

2.1 Preparation of Catalyst

HA material studied in this work was synthesized by precipitation method using a stoichiometric ratio of 1.67. Initially, two aqueous solutions containing 0.3 mol L^{-1} of $(NH_4)_2HPO_4$ and 0.5 mol L^{-1} of $Ca(NO_3)_2,4H_2O$ were prepared and their pH were adjusted to 11 using ammonia 24 %. The $(NH_4)_2HPO_4$ solution was drop-wisely added to the $Ca(NO_3)_2,4H_2O$ solution under vigorous stirring, while maintaining the pH at 11 using

ammonia. The mixture was then left under stirring at room temperature for 24 hours and the obtained precipitate was washed several times with distilled water. After drying at 100 °C overnight, the white precipitate was calcined for two hours at 120, 600 and 900 °C.

2.2 Characterization

X-ray powder diffraction (XRD) patterns were recorded on a Mini Diffractometer MD-10 equipped with Cu Kα radiation (λ = 1.5406 Å). Scanning electron microscopy image was performed on a JEOL JSM- 6360 LV emission scanning electron microscope (SEM) operating at 5.0 kV. The Fourier-transform infrared (FTIR) spectra were obtained using KBr technique on a JASCO-4100 FTIR spectrometer in the range of 400 to 4000 cm^{-1}.

2.3 Fenton-like catalytic reaction

The Fenton-like catalytic tests were carried out by adding a desired dose of HA material to 10 ml of MV dye solution with a chosen concentration. In order to determine the optimal conditions of the catalytic reaction, the effect of different parameters was investigated. The suspension was kept under stirring for 30 minutes to achieve adsorption/desorption equilibrium and then different doses of H_2O_2 were added into the reaction system. The optimal dose of H_2O_2 was then taken for all other catalytic tests. The pH of solution was adjusted to a desired value using 0.1 M H_2SO_4 or 0.5 M KOH aqueous solutions, and monitored online using a pH meter. The effect of temperature on the catalytic reaction was carried out in a cylindrical Pyrex double-walled reactor equipped with a thermostat. To identify the radical species responsible for the degradation of MV dye, tert-butanol (TBT) was added at different doses in the reaction solution as a scavenger. To determine the degradation efficiency, 3 mL of the suspension was collected and centrifuged at regular time intervals to separate the catalyst particles. Afterward, the obtained solution was analyzed by using a double-beam spectrophotometer (Jasco V-650) at maximum absorption wavelength of MV dye (λ_{max}= 582 nm). The degradation efficiency was calculated using the relation A_t / A_0, where A_t and A_0 are the maximum absorbance at time t and zero respectively.

3 RESULTS AND DISCUSSION

3.1 Catalyst Characterization

The X-ray diffractogram of the as synthetized material (Fig. 1-a) shows the reflection peaks of a pure hydroxyapatite crystallizing in the hexagonal system under space group $P6_3/m$, with $a = b = 9.41898$ Å; $c = 6.88119$ Å and $\alpha = \beta = 90°$; $\gamma = 120°$ as cell parameters according

to JCPDS card n°. 9-432. To study the effect of the synthesis temperature, the HA material was characterized by X-ray diffraction after each heat treatment at 120, 600 and 900 °C (Fig. 1-b) and the corresponding diffractograms confirm the presence of the apatitic structure with broad peaks for the material heated at 120 °C. With increasing temperature up to 600 °C, no change in diffraction peaks was observed. However, further increase to 900 °C revealed narrow peaks with a better resolution, likely due to improved crystallization. These results are in good agreement with other studies which show that an increase in the calcination temperature can control the grains morphology of hydroxyapatite and leads to well crystallized structures (Bensalah et al. 2018).

Fig. 1 Diffractogram of: (a) synthesized hydroxyapatite; (b) hydroxyapatite at different calcination temperatures

Recent studies have shown the existence of many morphologies for hydroxyapatites among them: cubic rods (Raghav et al. 2018), needle shape (Bensalah et al. 2018), agglomerated particles (Jastrzębski et al. 2011), microspheres (Yang et al. 2014) and others. These morphologies occur as a consequence of the elaboration method or following the variation of different parameters during the synthesis. For this purpose, we undertook to characterize the as-synthetized HA by the SEM technique. The micrography illustrated in Fig. 2 shows many agglomerates with mixed morphology. These agglomerates are composed from fine crystals whose sizes are less than 1 μm and other crystals in the form of platelets whose sizes are varying from 1 to 5 μm.

Fig. 2 SEM image of synthesized HA

The FTIR spectrum (Fig. 3) showed absorption bands at 1050 cm^{-1} attributed to the asymmetric stretching vibrations of the P-O bonds, while the peaks at 603 and 571 cm^{-1} are due to bending vibrations of O-P-O in phosphates groups (Roumila et al. 2018; Krukowski et al. 2018). The two peaks at 3670 cm^{-1} and 630 cm^{-1} are attributed to the OH group**s** of hydroxyapatite (Berzina-Cimdina and Borodajenko 2012). The spectrum shows a wide band around 3500 cm^{-1} and a peak at 1636 cm^{-1} corresponding respectively to the elongation and deformation vibrations of the O-H bonds in adsorbed water molecules (Wang et al. 2018).

Fig. 3 FTIR spectrum of $Ca_5(PO_4)_3OH$

3.2 Elimination of MV in different systems

The elimination of MV dye in various systems, namely, HA, H_2O_2, and HA+H_2O_2, was compared to study the catalytic activity of HA material in the HA/Fenton-like process. MV dye

degradation efficiency versus reaction time was shown in Fig. 4a. As it can be seen, about 20 % of MV dye was removed from the solution after 380 min either by oxidation with H_2O_2 system or by adsorption on HA material. These results indicated that the removal efficiency provided by both systems is too low to meet the practical needs of MV elimination. However, for the HA+H_2O_2 system, all of the MV dye was removed after 210 min, which indicates that the HA-catalyzed heterogeneous Fenton-like system was the main process for the elimination of MV pollutant. This result is well demonstrated by the absorption spectra of MV dye remaining in solution, that were recorded every 30 min (Fig. 4b). Indeed, these spectra show a decay of the main absorption band of MV dye, over time.

Fig. 4 (a) Comparison of the degradation efficiency of MV at 20 mg L^{-1} under various systems; (b) Absorption spectra of MV according to the Fenton-like process (T = 19 ± 2 °C, pH = 6.65, [MV] = 20 mg L^{-1}, HA dose = 2.5 g L^{-1} and [H_2O_2] = 12 mmol L^{-1})

3.3 Reaction mechanism

Despite its obvious importance, the mechanism of the Fenton or Fenton-like process reaction is not fully understood. The decomposition of hydrogen peroxide in our case could occur on the calcium sites present in the surface of catalyst according to the following equation:

$$\equiv Ca^{II} \text{ sites} + H_2O_2 \rightarrow \equiv Ca^{II} \text{ sites } H_2O_2 \quad (1)$$

$$\equiv Ca^{II} \text{ sites } H_2O_2 \rightarrow \equiv Ca^{I} \text{sites} + HO_2^{\bullet} + H^+ \quad (2)$$

$$\equiv Ca^{II} \text{sites} + HO_2^{\bullet} \rightarrow \equiv Ca^{I} \text{ sites} + O_2 + H^+ \quad (3)$$

$$\equiv Ca^{I} \text{ sites} + H_2O_2 \rightarrow \equiv Ca^{II} \text{ sites} + HO^{\bullet} + OH^- \quad (4)$$

To identify the main active species and to have a better understanding of the reaction pathway during the Fenton-like process, TBT is used as an efficient $HO^{\bullet}$ scavenger according to reaction (5) (Duesterberg and Waite 2006; Ding et al. 2016) :

$$C(CH_3)_3OH + HO^{\bullet} \longrightarrow C(CH_3)_3O^{\bullet} + H_2O \quad (5)$$

As demonstrated in Fig. 5, the efficiency degradation of MV is greatly influenced by the presence of the scavenger, where the efficiency decreases with increasing TBT concentration. The degraded MV amount in the presence of 0.27; 2 and 3 mol L^{-1} of the scavenger was found to be 68; 38 and 10 % respectively after 210 min, while the absence of the scavenger in the solution gives rise to a total elimination of MV. These results indicate that $HO^{\bullet}$ radicals are the main active species involved in the MV degradation process. Similar results are reported in the literature (Wan et al. 2017).

Fig. 5 Degradation of MV in the presence of TBT at different concentrations (T = 19 ± 2 °C, pH = 6.65, [MV] = 20 mg L^{-1}, HA dose = 2.5 g L^{-1}, [H_2O_2] = 12 mmol L^{-1})

3.4 Effect of the experimental parameters on the heterogeneous Fenton like process

The Fenton-like catalytic degradation of organic pollutants over HA particles is influenced by many reaction parameters such as H_2O_2 concentration, catalyst load, temperature and solution pH.

3.4.1 Effect of H_2O_2 concentration

The concentration of H_2O_2, source of $HO^{\bullet}$ radicals, can influence the Fenton-like process. Therefore, this parameter has been studied. The following curves (Fig. 6.) show remaining MV amount in solution as a function of time at different H_2O_2 concentrations.

Fig. 6 Effect of H_2O_2 concentration on MV dye degradation.
(T = 19 ± 2 °C, pH = 6.65, [MV] = 20 mg L^{-1}, HA dose = 2.5 g L^{-1}).

For each dose of H_2O_2 used, the amount of MV remaining in solution decreases gradually over time. When H_2O_2 concentration increases from 9 to 36 mmol L^{-1} the elimination rate increases. This result suggests that more $HO^{\bullet}$ radicals are formed which increased the MV dye degradation rate. However, when the H_2O_2 concentration is higher than 36 mmol L^{-1}, the degradation efficiency decreases. For example, at 300 mmol L^{-1} of H_2O_2, the degradation efficiency drops to 77 %. This decrease in the elimination rate is probably due to the consumption of the hydroxyl radicals $HO^{\bullet}$ by the excess of hydrogen peroxide according to the reaction (6), producing other radicals such as $O_2^{\bullet}$ and $HO_2^{\bullet}$, which have a lower oxidation capacity (Wang et al. 2014; Sun et al. 2018).

$$H_2O_2 + HO^{\bullet} \longrightarrow HO_2^{\bullet} \quad (6)$$

This study indicated that the optimal dosage of H_2O_2 is 36 mmol L^{-1}. Therefore, this latter concentration was chosen for the remainder of the study.

3.4.2 Effect of the Initial pH

pH is one of the most important factors influencing the Fenton or Fenton-like process. In general, the activity of heterogeneous Fenton catalysts is very limited at neutral and alkaline pH. To better study this effect, three pH values including the original one (pH = 6.65) were tested to degrade MV dye from solution, with an initial concentration of 20 mg L^{-1} and at a temperature of 19 ± 2 °C.

The curves illustrated in Fig. 7 show a progressive decrease in dye amount remaining in solution for each pH value. The results indicate that a total removal of MV dye from solution

was reached after 120 min at pH 6.65 against 150 min at pH 9.45. The slight drop in degradation efficiency observed at pH = 9.45 can be explained by the low oxidation potential of the hydroxyl radicals in basic medium (Ji et al. 2011). As for pH value around 5, a weak catalytic performance was observed probably due to the reactivity of the excess H^+ protons with the $HO^\bullet$ radicals, to form water molecules according to the reaction (7) (Wan et al. 2017). This is consistent with the increase in the pH value of the solution from 5 to 6.75 at the end of the catalytic reaction.

$$HO^\bullet + H^+ + e^- \longrightarrow H_2O \quad (7)$$

The experimental data indicated that the best degradation efficiency can be obtained at an optimized initial pH of 6.65.

Fig. 7 Effect of initial pH on MV degradation (T = 19 ± 2 °C, [MV] = 20 mg L^{-1}, [H_2O_2] = 36 mmol L^{-1}, HA dose = 2.5 g L^{-1})

3.4.3 Effect of Catalyst dose

We have already reported before that in the absence of HA catalyst, the degradation efficiency of MV is negligible (only 13 % after 210 min) (see section 3.2.1), highlighting the vital role of the HA catalyst in the Fenton-like process. To get inside this effect, several tests with different catalyst doses were carried out. The curves show that by increasing the catalyst dose from 0.75 to 2.5 g L^{-1}, a significant increase in the degradation efficiency is observed (Fig. 8). Indeed, when the HA dose goes from 0.75 to 2 g L^{-1}, the degradation efficiency increases from 21 to 50 % after 30 min. By increasing HA dosage to 2.5 g L^{-1}, a significant removal is achieved (82.7%) after 30 min and a total discoloration was obtained after 120 min. These results can be explained by the increase in the active sites due to the increase in the catalyst dose, which leads to a greater generation of $HO^\bullet$ radicals improving the degradation rate. Thus, 2.5 g L^{-1} HA is suitable for the reaction system.

Fig. 8 Effect of the catalyst dose on the degradation efficiency of MV (T = 19 ± 2 °C, pH = 6.65, [MV] = 20 mg L^{-1} and [H_2O_2] = 36 mmol L^{-1})

3.4.4 Effect of the reaction Temperature

The effect of reaction temperature on the MV solution discoloration was also studied. From Fig. 9 it can be seen that the degradation efficiency increased with the increase in reaction temperature. Indeed, MV dye is removed from the solution after 120 min at temperatures of 19 and 28 °C, after 60 min at 36 °C and after just 10 min at 48 °C In fact, a higher temperature increases the rate of reaction between the hydrogen peroxide and the catalyst, thus increasing

the rate of generation of the oxidizing species. In addition, a higher temperature can provide more energy to the system in the aim to overcome the reaction activation energy (Wang et al. 2014).

Fig. 9 Effect of temperature on MV degradation (pH = 6.65, [MV] = 20 mg L^{-1}, $[H_2O_2]$ = 36 mmol L^{-1}, HA dose = 2.5 g L^{-1})

3.4.5 Effect of the initial concentration of the MV solution

The degradation efficiency by the Fenton-like method on HA catalyst was studied at different concentrations of MV and the results are shown in Fig. 10.

Fig. 10 Effect of the initial concentration of MV solutions (T = 19 ± 2 °C, pH = 6.65, $[H_2O_2]$ = 36 mmol L^{-1} and HA dose = 2.5 g L^{-1})

Overall, it can be seen that as the initial MV concentration increases, the degradation efficiency decreases and the time required for total discoloration increases. The curves showed that all the MV dye was eliminated after 120 min at a concentration of 20 mg L^{-1} and 330 min at a concentration of 25 mg L^{-1}. On the other hand, this time was not sufficient to eliminate all the MV from the solution at a concentration of 30 mg L^{-1}. Similar behavior has been observed in other works on Fenton-like process (Park et al. 2018). The low degradation efficiency at high concentrations can be explained by the limited number of $HO^{\bullet}$ radicals in the reaction medium compared to the high number of MV molecules ([MV] > [$HO^{\bullet}$]). Therefore, under these experimental conditions, the percentage of generated $HO^{\bullet}$ radicals is insufficient to degrade all the dye molecules (Park et al. 2018).

3.5 Catalyst recycling tests

In order to assess the recycling efficiency as well as stability of the HA during the MV degradation, three cycles of Fenton-like process were carried out under the optimum conditions. After each experiment, the filtrate is removed and a new fresh solution of MV dye and H_2O_2 is added onto the same catalyst sample. The results showed that until the third cycle, the degradation efficiency remained effective with the same removal percentage (Fig.11).

Fig. 11 Catalyst recycling in MV degradation via a Fenton like process (T = 19 ± 2 °C, pH = 6.65, [MV] = 20 mg L^{-1}, $[H_2O_2]$ = 36 mmol L^{-1} and HA dose = 2.5 g L^{-1})

3.6 Kinetic studies

In order to study the degradation kinetics of MV dye by the Fenton-like process, three typical kinetic models were applied, i.e., the first-order, the second-order and the Behnajady-

Modirshahla-Ghanbery (BMG), as mathematically described by equations (8,9,10) respectively (Santana et al. 2019).

$$ln\frac{C_t}{C_0} = -k_1 t \quad (8)$$

$$\frac{1}{C_t} = \frac{1}{C_0} + k_2 t \quad (9)$$

$$\frac{t}{1-\frac{C_t}{C_0}} = m + bt \quad (10)$$

where, C_0 (mg L^{-1}) is the initial concentration of MV, C_t (mg L^{-1}) is the MV concentration at time t (min); k_1 (min^{-1}) is the rate constant for the first-order and k_2 (mg^{-1} L min^{-1}) is the rate constant for the second-order model; m (min) and b (dimensionless) are two characteristic constants for the BMG model that are related to reaction rates and oxidation capacity, respectively. The two parameters in BMG model are evaluated by examining time approaching zero or infinity, thus leading to the initial MV removal rate ($1/m$) and the theoretical maximum oxidation capacity of the catalyst ($1/b$). Accordingly, higher values of $1/m$ and $1/b$ indicate better catalytic performance. The fitted plots of the three kinetic models are shown in Supporting Information (Fig. S1, S2 and S3), while the obtained parameters are given in Table 1.

From these results, it could be seen that under the different reaction conditions, the values of the correlation factor in the first-order model and in the BMG model are closer to 1 as compared to those of the second order model. This implies that the experimental results are correctly described by the first order and BMG models. Indeed, the values of the different parameters of these models are in good agreement with experimental results as discussed below. For the influence of H_2O_2 concentration, the variation of k_1 and the two parameters $1/m$ and $1/b$ are shown in Supplementary Fig. S4a and Fig. S4b respectively. As seen in these figures, a sharp increase in k_1 and $1/m$ is observed when the H_2O_2 concentrations go from 9 to 36 mmol L^{-1}. However, k_1 and $1/m$ decreased when the concentration of H_2O_2 was higher than 36 mmol L^{-1}. This result can be explained by the lack of radicals in solution caused by the excess of H_2O_2 as reported in section 3.2.3.1. As for the oxidation capacity ($1/b$), it keeps the same values with a variance of ± 0.02 at each concentration of H_2O_2.

As it was demonstrated previously, the reaction rate is influenced by catalyst dosage. Practically, the increase in the HA dosage from 0.75 g L^{-1} to 2 g L^{-1} could increase the initial removal rate as illustrated in Supplementary Fig. S4C. Indeed, k_1 increased from 0.0037 to 0.015 min^{-1} and $1/m$ from 0.006 to 0.04 min^{-1}, and further increasing of the HA dose to 2.5 g L^{-1}, gives rise to the highest values of k_1 and $1/m$. In parallel, the oxidation capacity ($1/b$)

remains almost constant and ranging around the value of 1 to reach a maximum value of 1.08 at 1.5 g L-1 of HA dose and a minimum value of 0.92 at 1 g L-1 (Supplementary Fig. S4d).

The degradation rates (k_1 and $1/m$) and the maximum degradation capacity ($1/b$), as a function of initial pH, are shown in Supplementary Fig. S4e and Fig. S4f. It can be seen that the oxidation capacity ($1/b$) slightly increased while the removal rates (k_1 and $1/m$) increase by increasing pH from 5 to 6.65. However, at pH value over than 6.65 the removal rates decrease thus suggesting that the most favorable kinetic rate values can be obtained at an optimized initial pH of 6.65.

The kinetics of MV degradation at different reaction temperatures were also studied and represented in Supplementary Fig. S4g and Fig. S4h. From these figures, an increase in the value of the two removal rates (k_1 and $1/m$) is observed when the temperature goes from 20 to 36 °C, while the oxidation capacity keeps almost the same value. These results suggest that the mobility of the reactants was favored by the applied thermal energy as already discussed.

The kinetic rate is also influenced by the initial dye concentration. The curves in Supplementary Fig. S4i and Fig. S4j indicate that the initial removal rates (k_1 and $1/m$) decreased as increasing initial MV concentration and this is due to the increase in MV molecules compared to those of $HO^{\bullet}$ radicals generated in solution ([MV] > [$HO^{\bullet}$]). In fact, the concentration of H_2O_2 in the system was constant and equal to 36 mM thus fixing the number of radicals generated in the solution leading to an almost constant oxidation capacity $1/b$.

3.7 Thermodynamic studies

Based on the Arrhenius equation $k_1 = A\, exp\left(-\frac{E_a}{RT}\right)$ where k_1 is the rate constant, A is a pre-exponential factor, R is the universal gas constant (8.314 J mol^{-1} K^{-1}) and T is the temperature in K (Zhang et al. 2014), the activation energy (E_a) of the reaction was evaluated by plotting $ln\ k$ against $1/T$ (Fig. S5a in the Supporting Information). E_a was determined to be 30.72 kJ. mol^{-1} close to that reported by Suraj. P 2019 (Suraj et al. 2019). This value is higher than E_a of the diffusion-controlled reaction that usually ranges within 10–13 kJ mol^{-1}(Zubir et al. 2014) which implies that k_1 for this heterogeneous reaction is dominated by the rate of intrinsic chemical reactions on the surface of active sites rather than the rate of mass transfer as reported elsewhere (Xue et al. 2009).

The use of the theory of activated complexes developed by Eyring in 1930 (Khosroshahi and Mehrizad 2019) allowed us to calculate the enthalpy ($\Delta H°*$) and the entropy ($\Delta S°*$) of activation. The Eyring equation also called Eyring-Polanyi is given as follows:

$$k_1 = \frac{k_B T}{h}\ exp\left(-\frac{\Delta H^{\circ *}}{RT}\right)\ exp\left(\frac{\Delta S^{\circ *}}{R}\right) \quad (11)$$

where h is the Plank constant (6.62 10^{-34}J s^{-1}) and k_B the Boltzmann constant (1.38 $.10^{-23}$ J k^{-1}), $\Delta H^{\circ *}$ and $\Delta S^{\circ *}$ values were determined based on the slope and intercept of the ln (k_1 / T) versus (1/T) (Fig. S5b in the Supporting Information). Since the values of the free activation enthalpy $\Delta G^{\circ *}$ at different temperatures were calculated using the relationship of $\Delta G^{\circ *} = \Delta H^{\circ *}$ - $T\Delta S^{\circ *}$. The results obtained are reported in the following table:

According to the obtained results, the free activation enthalpy $\Delta G^{\circ *}$ is positive, which means that the Fenton-like reaction is non-spontaneous. The positive sign of the enthalpy suggests an endothermic process, which was predictable since the reaction was favored by a rise in temperature. The negative value of the entropy reflects and enhances regularity at the catalyst/solution interface during the Fenton-like reactions.

4 Conclusions

HA was prepared by precipitation method and characterized by many physicochemical techniques. The compound was used as a catalyst in a heterogeneous Fenton like process for the elimination of a cationic dye. At room temperature and neutral initial pH, a total removal was obtained within 120 min with HA dose of 2.5 g L^{-1}, H_2O_2 36 mmol L^{-1} and initial MV concentration of 20 mg L^{-1}. Furthermore, at 48 °C, a complete elimination was reached after just 10 min. The use of a scavenger highlighted the important role of HO• radicals in the process. The involved process was evaluated by both kinetic and thermodynamic studies. The results revealed that the kinetic rate follows the first-order and BMG kinetic models, where the removal rate increases by increasing H_2O_2 concentration, catalyst dosage and temperature. A good correlation was observed between empirical and modelled data. The thermodynamic parameters indicated a non-spontaneous and endothermic process. Based on the findings of the present research, HA catalyst would have potential applications in the field of wastewater treatment due to its non-toxicity, chemical stability, good catalytic activity and easy recycling.

Supplementary Information The online version contains supplementary material.

Acknowledgments

The authors thank MHESR (Ministry of Higher Education and Scientific Research) Algeria, for the financial support.

Author contribution: All authors contributed to the study conception and design. Material preparation, data collection, and analysis were performed by Y. Roumila, S. Debaghi and D. Meziani. The manuscript was written by Y. Roumila and D. Meziani. K. Abdmeziem supervised all of the work and contributed to the writing and editing of the manuscript. All authors read and approved the final manuscript.

Availability of data and material Not applicable.

Declarations

Ethical approval Not applicable.

Consent to participate Not applicable.

Consent for publication Not applicable.

Competing interests The authors declare no competing interests

References

Ajoudanian N, Nezamzadeh-Ejhieh A (2015) Enhanced photocatalytic activity of nickel oxide supported on clinoptilolite nanoparticles for the photodegradation of aqueous cephalexin. Mater Sci Semicond Process 36:162–169. https://doi.org/10.1016/j.mssp.2015.03.042

Babuponnusami A, Muthukumar K (2014) A review on Fenton and improvements to the Fenton process for wastewater treatment. J Environ Chem Eng 2:557–572. https://doi.org/10.1016/j.jece.2013.10.011

Bello MM, Abdul Raman AA, Asghar A (2019) A review on approaches for addressing the limitations of Fenton oxidation for recalcitrant wastewater treatment. Process Saf Environ Prot 126:119–140. https://doi.org/10.1016/j.psep.2019.03.028

Bensalah H, Bekheet MF, Alami Younssi S, et al (2018) Hydrothermal synthesis of nanocrystalline hydroxyapatite from phosphogypsum waste. J Environ Chem Eng 6:1347–1352. https://doi.org/10.1016/j.jece.2018.01.052

Berkessa YW, Yan B, Li T, et al (2020) Treatment of anthraquinone dye textile wastewater using anaerobic dynamic membrane bioreactor: Performance and microbial dynamics. Chemosphere 238:124539. https://doi.org/10.1016/j.chemosphere.2019.124539

Berzina-Cimdina L, Borodajenko N (2012) Research of Calcium Phosphates Using Fourier

411 Transform Infrared Spectroscopy. In: Infrared Spectroscopy - Materials Science,
412 Engineering and Technology. InTech, pp 123–148
413 Bilińska L, Blus K, Foszpańczyk M, et al (2020) Catalytic ozonation of textile wastewater as
414 a polishing step after industrial scale electrocoagulation. J Environ Manage 265:110502.
415 https://doi.org/10.1016/j.jenvman.2020.110502
416 Ciobanu G, Harja M (2019) Cerium-doped hydroxyapatite/collagen coatings on titanium for
417 bone implants. Ceram Int 45:2852–2857. https://doi.org/10.1016/j.ceramint.2018.07.290
418 Ding Y, Huang W, Ding Z, et al (2016) Dramatically enhanced Fenton oxidation of
419 carbamazepine with easily recyclable microscaled $CuFeO_2$ by hydroxylamine: Kinetic
420 and mechanism study. Sep Purif Technol 168:223–231.
421 https://doi.org/10.1016/j.seppur.2016.05.043
422 Dong X, Lin Y, Ren G, et al (2021) Catalytic Degradation of Methylene Blue by Fenton-like
423 Oxidation of Ce-doped MOF. Colloids Surfaces A Physicochem Eng Asp 608:125578.
424 https://doi.org/10.1016/j.colsurfa.2020.125578
425 Duesterberg CK, Waite TD (2006) Process optimization of fenton oxidation using kinetic
426 modeling. Environ Sci Technol 40:4189–4195. https://doi.org/10.1021/es060311v
427 Fida H, Zhang G, Guo S, Naeem A (2017) Heterogeneous Fenton degradation of organic
428 dyes in batch and fixed bed using La-Fe montmorillonite as catalyst. J Colloid Interface
429 Sci 490:859–868. https://doi.org/10.1016/j.jcis.2016.11.085
430 Fihri A, Len C, Varma RS, Solhy A (2017) Hydroxyapatite: A review of syntheses, structure
431 and applications in heterogeneous catalysis. Coord Chem Rev 347:48–76.
432 https://doi.org/10.1016/j.ccr.2017.06.009
433 Gonzalez-Olmos R, Holzer F, Kopinke FD, Georgi A (2011) Indications of the reactive
434 species in a heterogeneous Fenton-like reaction using Fe-containing zeolites. Appl Catal
435 A Gen 398:44–53. https://doi.org/10.1016/j.apcata.2011.03.005
436 Harja M, Ciobanu G (2018) Studies on adsorption of oxytetracycline from aqueous solutions
437 onto hydroxyapatite. Sci Total Environ 628–629:36–43.
438 https://doi.org/10.1016/j.scitotenv.2018.02.027
439 Hassan H, Hameed BH (2011) Fe–clay as effective heterogeneous Fenton catalyst for the
440 decolorization of Reactive Blue 4. Chem Eng J 171:912–918.
441 https://doi.org/10.1016/j.cej.2011.04.040
442 He X, Qi Z, Gao J, et al (2020) Nonylphenol ethoxylates biodegradation increases
443 estrogenicity of textile wastewater in biological treatment systems. Water Res
444 184:116137. https://doi.org/10.1016/j.watres.2020.116137

445 Ikhsan SNW, Yusof N, Ismail AF, et al (2020) Synthetic polymer-based membranes for
446 treatment of oily wastewater. In: Synthetic Polymeric Membranes for Advanced Water
447 Treatment, Gas Separation, and Energy Sustainability. Elsevier, pp 3–22
448 Jastrzębski W, Sitarz M, Rokita M, Bułat K (2011) Infrared spectroscopy of different
449 phosphates structures. Spectrochim Acta Part A Mol Biomol Spectrosc 79:722–727.
450 https://doi.org/10.1016/j.saa.2010.08.044
451 Ji F, Li C, Zhang J, Deng L (2011) Efficient decolorization of dye pollutants with
452 LiFe(WO4)2 as a reusable heterogeneous Fenton-like catalyst. Desalination 269:284–
453 290. https://doi.org/10.1016/j.desal.2010.11.015
454 Khan S, Malik A, Akhtar R, Grohmann E (2014) Environmental Deterioration and Human
455 Health. In: Malik A, Grohmann E, Akhtar R (eds) Environmental Deterioration and
456 Human Health: Natural and Anthropogenic Determinants. Springer Netherlands,
457 Dordrecht, pp 55–71
458 Khosroshahi AG, Mehrizad A (2019) Optimization, kinetics and thermodynamics of
459 photocatalytic degradation of Acid Red 1 by Sm-doped CdS under visible light. J Mol
460 Liq 275:629–637. https://doi.org/10.1016/j.molliq.2018.11.122
461 Kiani R, Mirzaei F, Ghanbari F, et al (2020) Real textile wastewater treatment by a sulfate
462 radicals-Advanced Oxidation Process: Peroxydisulfate decomposition using copper
463 oxide (CuO) supported onto activated carbon. J Water Process Eng 38:101623.
464 https://doi.org/10.1016/j.jwpe.2020.101623
465 Krukowski S, Lysenko N, Kolodziejski W (2018) Synthesis and characterization of
466 nanocrystalline composites containing calcium hydroxyapatite and glycine. J Solid State
467 Chem 264:59–67. https://doi.org/10.1016/j.jssc.2018.05.004
468 Lan Y, Barthe L, Azais A, Causserand C (2020) Feasibility of a heterogeneous Fenton
469 membrane reactor containing a Fe-ZSM5 catalyst for pharmaceuticals degradation:
470 Membrane fouling control and long-term stability. Sep Purif Technol 231:115920.
471 https://doi.org/10.1016/j.seppur.2019.115920
472 Lellis B, Fávaro-Polonio CZ, Pamphile JA, Polonio JC (2019) Effects of textile dyes on
473 health and the environment and bioremediation potential of living organisms. Biotechnol
474 Res Innov 3:275–290. https://doi.org/10.1016/j.biori.2019.09.001
475 Long Q, Liu F, Yuan Y, et al (2020) Enhanced degradation performance of p-chlorophenol in
476 photo-Fenton reaction activated by nano-Fe0 encapsulated in hydrothermal carbon:
477 Improved Fe(III)/Fe(II) cycle. Colloids Surfaces A Physicochem Eng Asp 594:124650.
478 https://doi.org/10.1016/j.colsurfa.2020.124650

Meziani D, Abdmeziem K, Bouacida S, et al (2016) Photo-electrochemical and physical characterizations of a new single crystal POM- based material. Application to Rhodamine B photodegradation. Sol Energy Mater Sol Cells 147:46–52. https://doi.org/10.1016/j.solmat.2015.11.042

Mortadi A, Chahid EG, Elmelouky A, et al (2020) Complex electrical conductivity as a new technique to monitor the coagulation-flocculation processes in the wastewater treatment of the textile Industry. Water Resour Ind 24:100130. https://doi.org/10.1016/j.wri.2020.100130

Nishikawa H (2004) A high active type of hydroxyapatite for photocatalytic decomposition of dimethyl sulfide under UV irradiation. J Mol Catal A Chem 207:149–153. https://doi.org/10.1016/S1381-1169(03)00472-2

Oliva J, De Pablo J, Cortina J-L, et al (2011) Removal of cadmium, copper, nickel, cobalt and mercury from water by Apatite II^{TM}: Column experiments. J Hazard Mater 194:312–323. https://doi.org/10.1016/j.jhazmat.2011.07.104

Ooi CH, Ling YP, Pung SY, Yeoh FY (2019) Mesoporous hydroxyapatite derived from surfactant-templating system for p-Cresol adsorption: Physicochemical properties, formation process and adsorption performance. Powder Technol 342:725–734. https://doi.org/10.1016/j.powtec.2018.10.043

Oulguidoum A, Bouyarmane H, Laghzizil A, et al (2019) Development of sulfonate-functionalized hydroxyapatite nanoparticles for cadmium removal from aqueous solutions. Colloids Interface Sci Commun 30:100178. https://doi.org/10.1016/j.colcom.2019.100178

Park JH, Wang JJ, Xiao R, et al (2018) Degradation of Orange G by Fenton-like reaction with Fe-impregnated biochar catalyst. Bioresour Technol 249:368–376. https://doi.org/10.1016/j.biortech.2017.10.030

Raghav S, Sapna, Kumar D (2018) Cubical-Shaped Rods of Pectin-Hydroxyapatite Composite for Adsorption Studies of Fluoride by Statistical Method and Adsorption Experiments. ACS Omega 3:9675–9688. https://doi.org/10.1021/acsomega.8b01330

Riaz M, Zia R, Ijaz A, et al (2018) Synthesis of monophasic Ag doped hydroxyapatite and evaluation of antibacterial activity. Mater Sci Eng C 90:308–313. https://doi.org/10.1016/j.msec.2018.04.076

Roumila Y, Abdmeziem K, Meziani D, Trari M (2018) Physical and photo-electrochemical characterization of natural phosphate material. Application to basic dyes photodegradation. Res Chem Intermed 44:2621–2636. https://doi.org/10.1007/s11164-

513 018-3250-2
514 Roumila Y, Abdmeziem K, Rekhila G, Trari M (2016) Semiconducting properties of
515 hydrothermally synthesized libethenite application to orange G photodegradation. Mater
516 Sci Semicond Process 41:470–479. https://doi.org/10.1016/j.mssp.2015.10.018
517 Saber A, Smahi A, Solhy A, et al (2003) Heterogeneous catalysis of Friedel-Crafts alkylation
518 by the fluorapatite alone and doped with metal halides. J Mol Catal A Chem 202:229–
519 237. https://doi.org/10.1016/S1381-1169(03)00186-9
520 Sangeetha K, Ashok M, Girija EK, et al (2018) Strontium and ciprofloxacin modified
521 hydroxyapatites as functional grafts for bone prostheses. Ceram Int 44:13782–13789.
522 https://doi.org/10.1016/j.ceramint.2018.04.221
523 Santana CS, Nicodemos Ramos MD, Vieira Velloso CC, Aguiar A (2019) Kinetic Evaluation
524 of Dye Decolorization by Fenton Processes in the Presence of 3-Hydroxyanthranilic
525 Acid. Int J Environ Res Public Health 16:1602. https://doi.org/10.3390/ijerph16091602
526 Sebatini S, Kalluri S, Anish Madhavan A (2020) Green synthesized α-Fe_2O_3 mesoporous
527 network for heterogeneous Fenton oxidation of thiazine dye. Mater Lett X 5:100037.
528 https://doi.org/10.1016/j.mlblux.2019.100037
529 Sebti S, Solhy A, Tahir R, Smahi A (2002) Modified hydroxyapatite with sodium nitrate: An
530 efficient new solid catalyst for the Claisen-Schmidt condensation. Appl Catal A Gen
531 235:273–281. https://doi.org/10.1016/S0926-860X(02)00273-9
532 Sun B, Li H, Li X, et al (2018) Degradation of Organic Dyes over Fenton-Like Cu_2O-Cu/C
533 Catalysts. Ind Eng Chem Res 57:14011–14021. https://doi.org/10.1021/acs.iecr.8b02697
534 Suraj P, Kumar V, Thakur C, Ghosh P (2019) Taguchi optimization of COD removal by
535 heterogeneous Fenton process using copper ferro spinel catalyst in a fixed bed reactor -
536 RTD, kinetic and thermodynamic study. J Environ Chem Eng 7:102859.
537 https://doi.org/10.1016/j.jece.2018.102859
538 Tang X, Li Z, Liu K, et al (2020) Sulfidation modified Fe_3O_4 nanoparticles as an efficient
539 Fenton-like catalyst for azo dyes degradation at wide pH range. Powder Technol
540 376:42–51. https://doi.org/10.1016/j.powtec.2020.08.018
541 Vahdat A, Ghasemi B, Yousefpour M (2019) Synthesis of hydroxyapatite and
542 hydroxyapatite/Fe_3O_4 nanocomposite for removal of heavy metals. Environ
543 Nanotechnology, Monit Manag 12:100233. https://doi.org/10.1016/j.enmm.2019.100233
544 Venkateswarlu K, Chandra Bose A, Rameshbabu N (2010) X-ray peak broadening studies of
545 nanocrystalline hydroxyapatite by Williamson–Hall analysis. Phys B Condens Matter
546 405:4256–4261. https://doi.org/10.1016/j.physb.2010.07.020

547 Wan W, Zhang Y, Ji R, et al (2017) Metal Foam-Based Fenton-Like Process by Aeration.
548 ACS Omega 2:6104–6111. https://doi.org/10.1021/acsomega.7b00977
549 Wang J, Gong X, Hai J, Li T (2018) Synthesis of silver–hydroxyapatite composite with
550 improved antibacterial properties. Vacuum 152:132–137.
551 https://doi.org/10.1016/j.vacuum.2018.03.015
552 Wang N, Zheng T, Zhang G, Wang P (2016) A review on Fenton-like processes for organic
553 wastewater treatment. J Environ Chem Eng 4:762–787.
554 https://doi.org/10.1016/j.jece.2015.12.016
555 Wang Q, Tian S, Ning P (2014) Degradation Mechanism of Methylene Blue in a
556 Heterogeneous Fenton-like Reaction Catalyzed by Ferrocene. Ind Eng Chem Res
557 53:643–649. https://doi.org/10.1021/ie403402q
558 Wu J, Doan H, Upreti S (2008) Decolorization of aqueous textile reactive dye by ozone.
559 Chem Eng J 142:156–160. https://doi.org/10.1016/j.cej.2007.11.019
560 Xue X, Hanna K, Abdelmoula M, Deng N (2009) Adsorption and oxidation of PCP on the
561 surface of magnetite: Kinetic experiments and spectroscopic investigations. Appl Catal
562 B Environ 89:432–440. https://doi.org/10.1016/j.apcatb.2008.12.024
563 Yang Y, Wu Q, Wang M, et al (2014) Hydrothermal Synthesis of Hydroxyapatite with
564 Different Morphologies: Influence of Supersaturation of the Reaction System. Cryst
565 Growth Des 14:4864–4871. https://doi.org/10.1021/cg501063j
566 Zahouily M, Abrouki Y, Bahlaouan B, et al (2003) Hydroxyapatite: new efficient catalyst for
567 the Michael addition. Catal Commun 4:521–524.
568 https://doi.org/10.1016/j.catcom.2003.08.001
569 Zárate-Guzmán AI, González-Gutiérrez L V., Ocampo-Pérez R, et al (2020) Iron precursor
570 salt effect on the generation of OH radicals and sulfamethoxazole degradation through a
571 heterogeneous Fenton process using Carbon-Fe catalysts. J Water Process Eng
572 36:101273. https://doi.org/10.1016/j.jwpe.2020.101273
573 Zaviska F, Drogui P, Mercier G, Blais J-F (2009) Procédés d'oxydation avancée dans le
574 traitement des eaux et des effluents industriels: Application à la dégradation des
575 polluants réfractaires. Rev des Sci l'eau 22:535–564. https://doi.org/10.7202/038330ar
576 Zhang Q, Wang Q, Wang S (2020) Efficient heterogeneous Fenton-like catalysis of Fe-doped
577 SAPO-44 zeolite synthesized from bauxite and rice husk. Chem Phys Lett 753:137598.
578 https://doi.org/10.1016/j.cplett.2020.137598
579 Zhang X, Ding Y, Tang H, et al (2014) Degradation of bisphenol A by hydrogen peroxide
580 activated with $CuFeO_2$ microparticles as a heterogeneous Fenton-like catalyst:

Efficiency, stability and mechanism. Chem Eng J 236:251–262. https://doi.org/10.1016/j.cej.2013.09.051

Zhou Y, Zhang Y, Li Z, et al (2020) Oxygen reduction reaction electrocatalysis inducing Fenton-like processes with enhanced electrocatalytic performance based on mesoporous ZnO/CuO cathodes: Treatment of organic wastewater and catalytic principle. Chemosphere 259:127463. https://doi.org/10.1016/j.chemosphere.2020.127463

Zubir NA, Yacou C, Zhang X, Diniz da Costa JC (2014) Optimisation of graphene oxide–iron oxide nanocomposite in heterogeneous Fenton-like oxidation of Acid Orange 7. J Environ Chem Eng 2:1881–1888. https://doi.org/10.1016/j.jece.2014.08.001

Figures

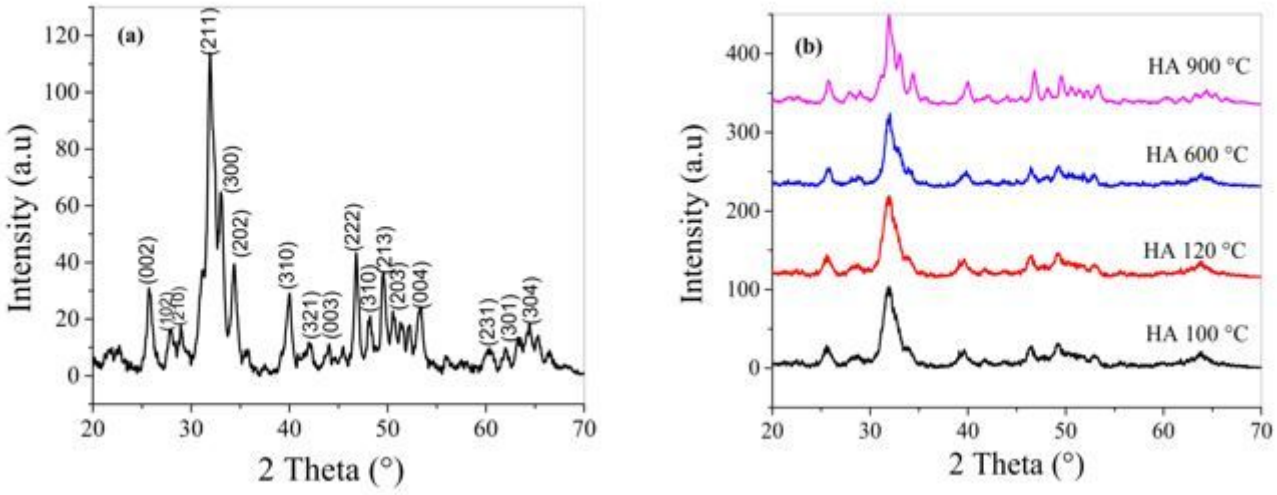

Figure 1

Diffractogram of: (a) synthesized hydroxyapatite; (b) hydroxyapatite at different calcination temperatures

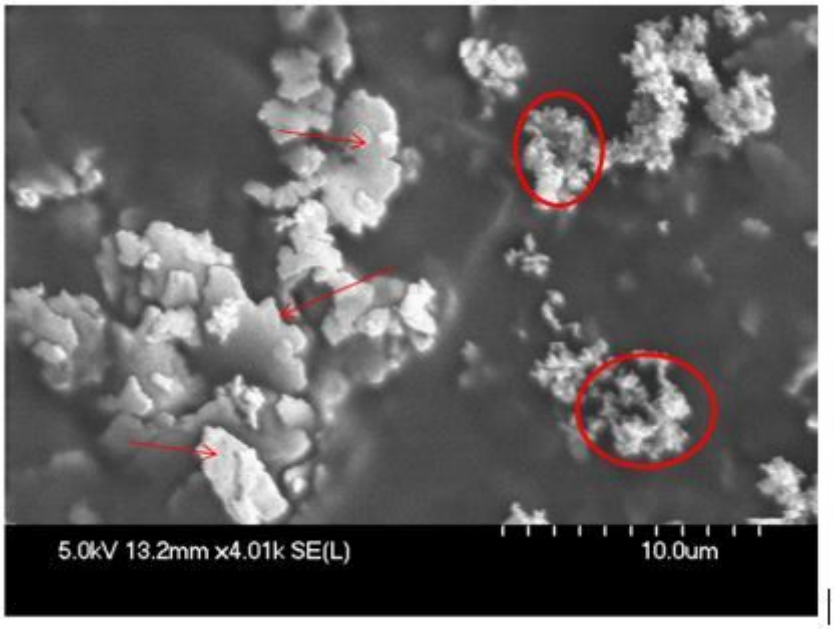

Figure 2

SEM image of synthesized HA

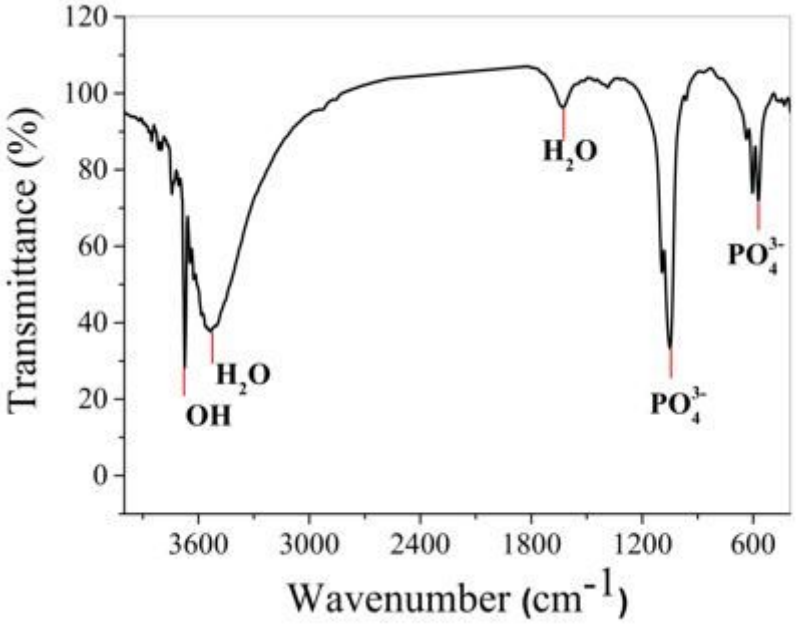

Figure 3

FTIR spectrum of Ca5(PO4)3OH

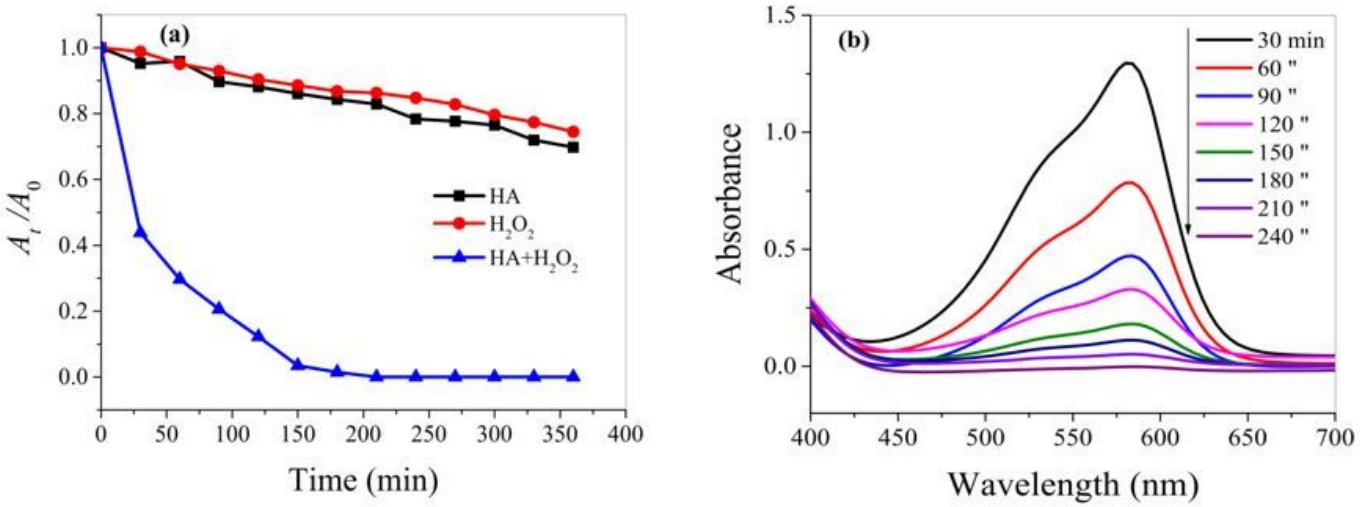

Figure 4

(a) Comparison of the degradation efficiency of MV at 20 mg L-1 under various systems; (b) Absorption spectra of MV according to the Fenton-like process (T = 19 ± 2 °C, pH = 6.65, [MV] = 20 mg L-1, HA dose = 2.5 g L-1 and [H2O2] = 12 mmol L-1)

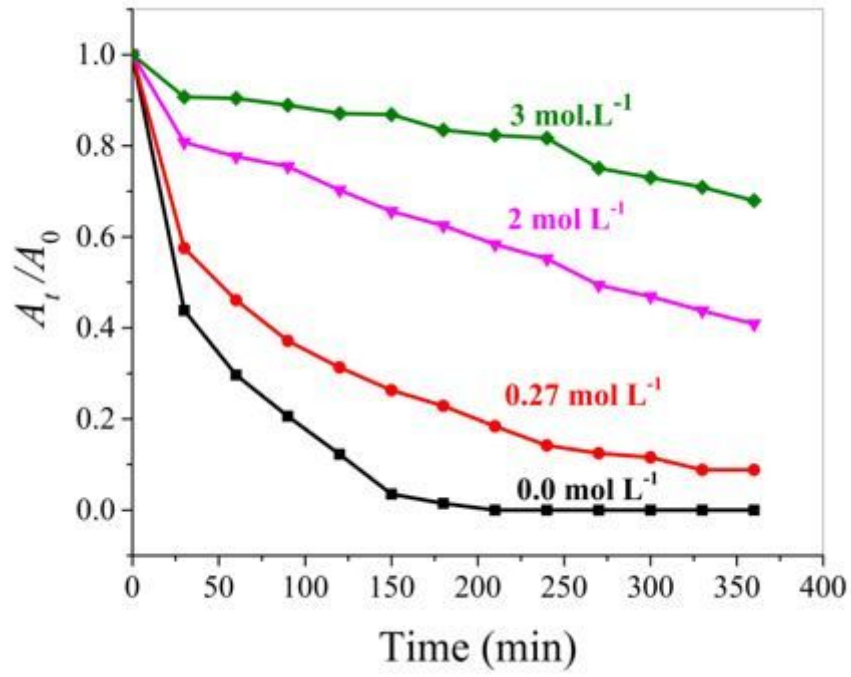

Figure 5

Degradation of MV in the presence of TBT at different concentrations (T = 19 ± 2 °C, pH = 6.65, [MV] = 20 mg L-1, HA dose = 2.5 g L-1, [H2O2] = 12 mmol L-1)

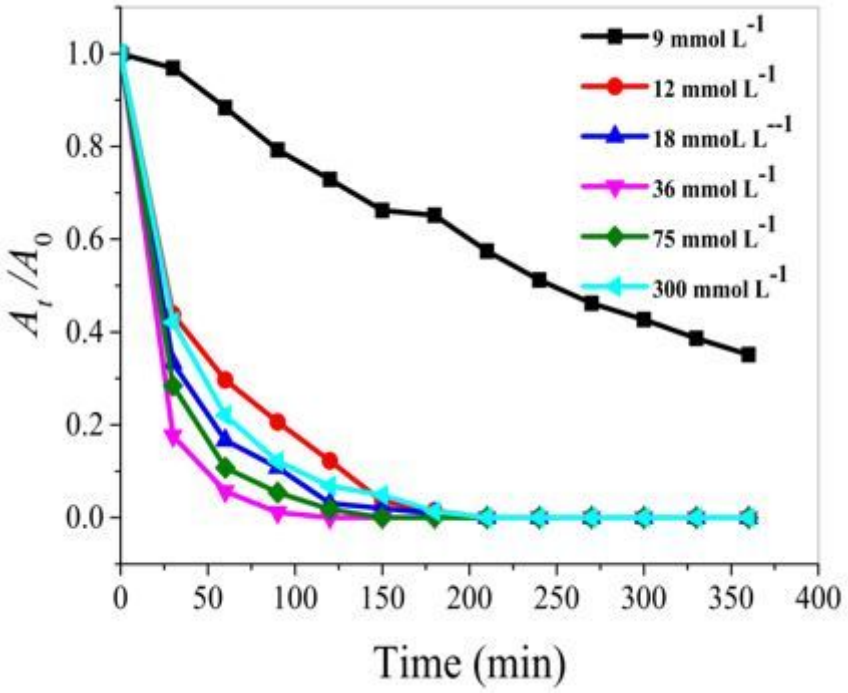

Figure 6

Effect of H2O2 concentration on MV dye degradation. (T = 19 ± 2 °C, pH = 6.65, [MV] = 20 mg L-1, HA dose = 2.5 g L-1).

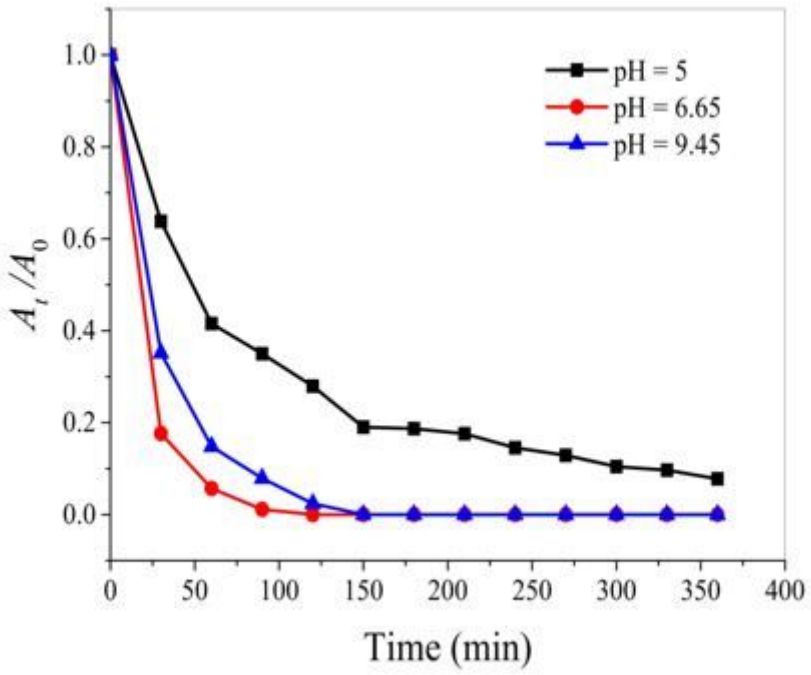

Figure 7

Effect of initial pH on MV degradation (T = 19 ± 2 °C, [MV] = 20 mg L-1, [H2O2] = 36 mmol L-1, HA dose = 2.5 g L-1)

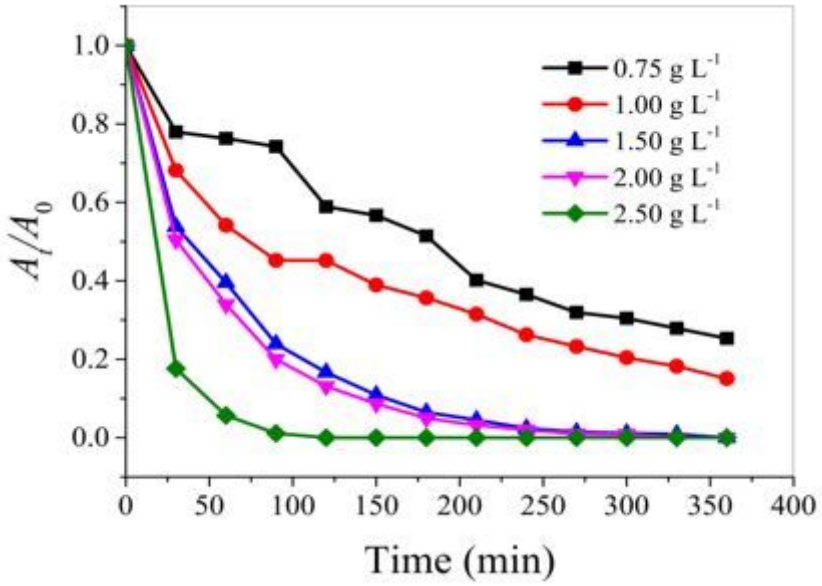

Figure 8

Effect of the catalyst dose on the degradation efficiency of MV (T = 19 ± 2 °C, pH = 6.65, [MV] = 20 mg L-1 and [H2O2] = 36 mmol L-1)

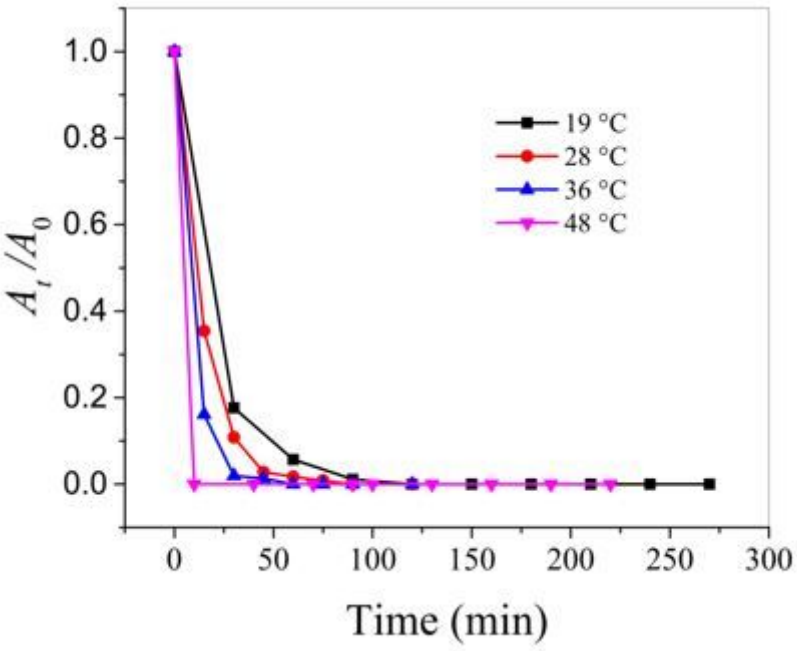

Figure 9

Effect of temperature on MV degradation (pH = 6.65, [MV] = 20 mg L-1, [H2O2] = 36 mmol L-1, HA dose = 2.5 g L-1)

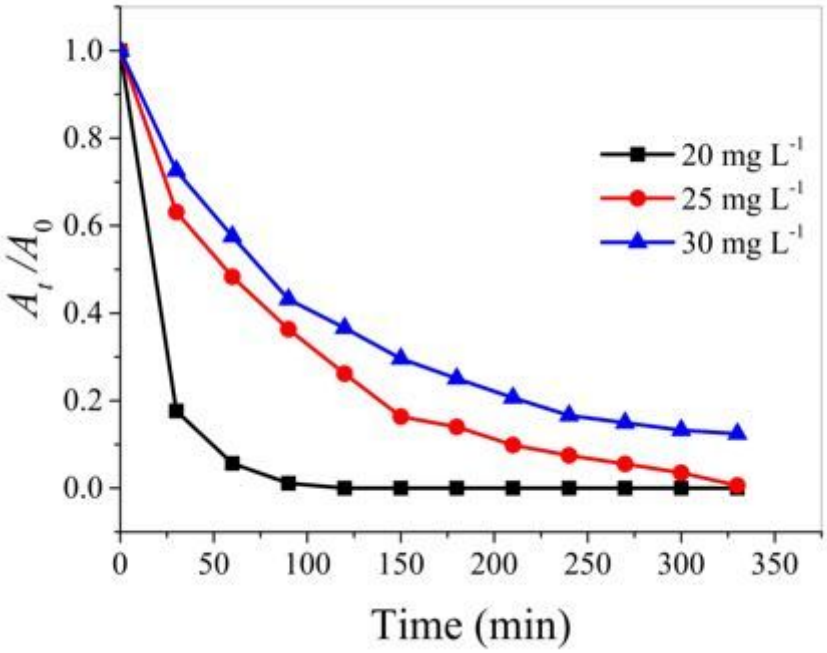

Figure 10

Effect of the initial concentration of MV solutions (T = 19 ± 2 °C, pH = 6.65, [H2O2] = 36 mmol L-1 and HA dose = 2.5 g L-1)

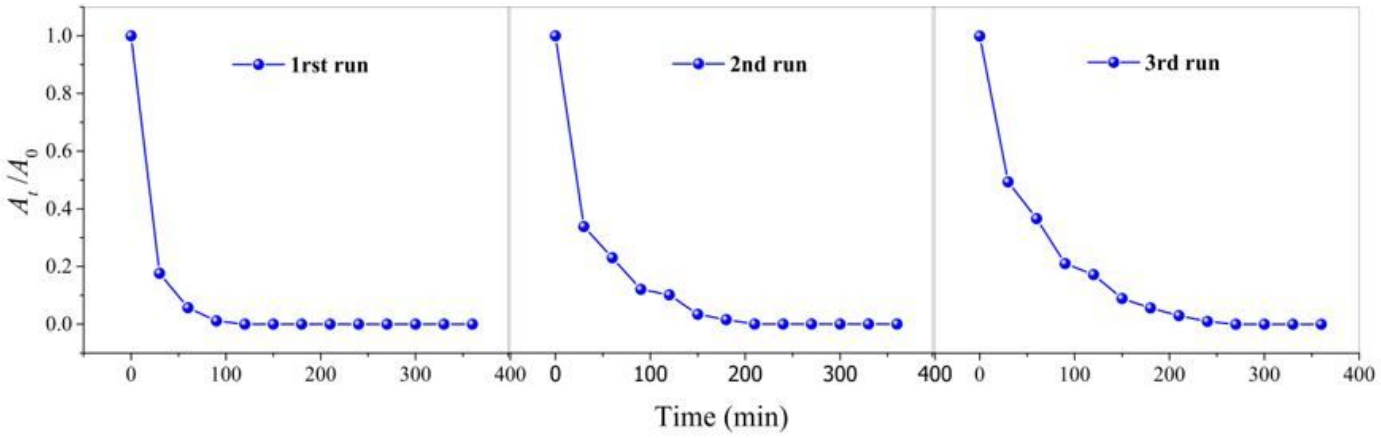

Figure 11

Catalyst recycling in MV degradation via a Fenton like process (T = 19 ± 2 °C, pH = 6.65, [MV] = 20 mg L-1, [H2O2] = 36 mmol L-1 and HA dose = 2.5 g L-1)

Supplementary Files

This is a list of supplementary files associated with this preprint. Click to download.

- Supplementarymaterial.docx